

JGR Atmospheres

RESEARCH ARTICLE

10.1029/2022JD038184

Key Points:

- Urban expansion and anthropogenic heat (AH) enhancement impact tropical cyclone precipitation (TCP) in the Greater Bay Area (GBA), China
- Both AH enhancement and urban expansion can boost TCP in urban areas, while only AH enhancement favors TCP in urban downstream areas
- AH enhancement and urban expansion impact TCP mainly by affecting low-level moisture convergence

Supporting Information:

Supporting Information may be found in the online version of this article.

Correspondence to:

Q. Li,
ql.li@siat.ac.cn

Citation:

He, L., Li, Q., Wang, Y., Lee, J. H. W., Xu, Y., & Li, G. (2023). Effects of urban expansion and anthropogenic heat enhancement on tropical cyclone precipitation in the Greater Bay Area of China. *Journal of Geophysical Research: Atmospheres*, 128, e2022JD038184.
<https://doi.org/10.1029/2022JD038184>

Received 13 NOV 2022

Accepted 21 JUL 2023

Author Contributions:

Conceptualization: Lunkai He, Qinglan Li, Yuqing Wang, Joseph H. W. Lee, Yinglong Xu

Data curation: Lunkai He

Formal analysis: Lunkai He

Funding acquisition: Qinglan Li

Investigation: Lunkai He, Qinglan Li

Methodology: Lunkai He, Qinglan Li

Project Administration: Qinglan Li

Resources: Qinglan Li, Yinglong Xu

Software: Lunkai He

Supervision: Qinglan Li

Validation: Lunkai He

Visualization: Lunkai He, Qinglan Li, Guangxin Li

Writing – original draft: Lunkai He, Qinglan Li, Yuqing Wang

Writing – review & editing: Qinglan Li, Yuqing Wang, Joseph H. W. Lee, Yinglong Xu, Guangxin Li

© 2023. American Geophysical Union.
All Rights Reserved.

Effects of Urban Expansion and Anthropogenic Heat Enhancement on Tropical Cyclone Precipitation in the Greater Bay Area of China

Lunkai He^{1,2}, Qinglan Li¹ , Yuqing Wang³ , Joseph H. W. Lee⁴ , Yinglong Xu⁵, and Guangxin Li¹

¹Shenzhen Institute of Advanced Technology, Chinese Academy of Sciences, Shenzhen, China, ²University of Chinese Academy of Sciences, Beijing, China, ³Department of Atmospheric Sciences, International Pacific Research Center, School of Ocean and Earth Science and Technology, University of Hawaii at Manoa, Honolulu, HI, USA, ⁴Macau Environmental Research Institute, Macau University of Science and Technology, Macau, China, ⁵National Meteorological Center, Beijing, China

Abstract The impact of urban expansion and anthropogenic heat (AH) enhancement on tropical cyclone precipitation (TCP) in the Guangdong–Hong Kong–Macau Greater Bay Area (GBA) of China is investigated by using the Weather Research and Forecasting (WRF) model. Sensitivity experiments are conducted during the landfall periods of two tropical cyclones, Hato (2017) and Mangkhut (2018), by artificially varying the surface AH flux from 0 to 600 W/m² and the urban land surface from 1985 to 2017, respectively. Results show that the TCP in the GBA's urban region increases with both urban expansion and AH enhancement. However, in the urban downstream region, only AH enhancement causes an increase in TCP, whereas urban expansion has no significant influence on TCP. AH enhancement and urban expansion affect surface temperature, surface sensible heat flux, and surface latent heat flux, leading to changes in atmospheric instability and surface water evaporation, resulting in changes in low-level moisture convergence. The change patterns of the vertically integrated moisture flux divergence between 850 and 910 hPa in the urban and urban downstream regions of the GBA are consistent with those of the TCP changes in this area, indicating that low-level moisture convergence is the key factor determining the TCP changes in the region.

Plain Language Summary This study examines the impact of urban expansion and anthropogenic heat (AH) enhancement on tropical cyclone precipitation (TCP) in the Guangdong–Hong Kong–Macau Greater Bay Area. Through sensitivity experiments by the Weather Research and Forecasting model, we find that both urban expansion and AH enhancement increase TCP in the urban region. However, AH enhancement favors TCP in the urban downstream region, whereas urban expansion has no significant influence on TCP in the region. Further analysis reveals that urban expansion and AH enhancement determine the TCP changes mainly by affecting low-level moisture convergence, represented by the vertically integrated moisture flux convergence between 850 and 910 hPa.

1. Introduction

Tropical cyclone precipitation (TCP) is influenced not only by large-scale environmental factors and tropical cyclone (TC) severity, but also by local topography and urbanization (Palumbo & Mazzarella, 1980). Urban expansion is usually accompanied by rapid land-use alteration in the surface topography, resulting in changes in thermal conductivity, hydraulic permeability, and other properties in urban areas (Y. Li et al., 2021; C. L. Zhang et al., 2009). These changes can lead to variations in energy balance, affecting the surface wind, mixing layer depth, and thermal structures of the boundary layer (Demuzere et al., 2013; Grawe et al., 2013), potentially leading to more frequent extreme rainfall events and other disasters in urbanized areas (Yan et al., 2020; L. Yang et al., 2014).

Based on observational data and numerical model simulations, many studies have investigated how urbanization impacts the precipitation intensity, amount, and spatial patterns in and near large cities. Urbanization may increase precipitation in the urban upstream or downstream area (Changnon, 1979; Lin et al., 2011; Xiao et al., 2020; Y. Zhang et al., 2017), and the effect of urbanization on moderate and heavy convective precipitation is particularly significant (Gero & Pitman, 2006; Kusaka et al., 2014; M. Zhang, 2015).

By analyzing Tropical Rainfall Measuring Mission (TRMM) data from January 1998 to May 2002, Shepherd and Burian (2003) discovered that the strongest annual mean precipitation occurred mainly in the downstream area of Houston. Over coastal urban areas, such as Osaka Kinki and the Tokyo metropolitan regions, there was stronger and more frequent extreme rainfall (Kusaka et al., 2014; Shimadera et al., 2015; Xiao et al., 2020). According to a quantitative meta-analysis assessment of 85 studies from 48 papers, J. Liu and Niyogi (2019) indicated that urbanization could increase precipitation intensity by 11% (14%) to 21% (22%) in the urban (urban downstream) area, but only slightly in other areas. Strong Urban Heat Island (UHI) could increase rainfall directly over Beijing's downtown area, whereas weak UHI caused rainfall to be bifurcated and avoid the city center (Dou et al., 2015; Y. Zhang et al., 2017). Based on station data and satellite reanalysis, urban expansion was found to result in stronger and more frequent extreme rainfall events over the Guangdong–Hong Kong–Macau Greater Bay Area (GBA) in recent years (J. Wang et al., 2015). By historical observations, the rainfall center in Shenzhen was found to locate downstream of the urban region (X. Lu et al., 2019). The downstream of the urban area was also the rainfall center in Guangdong Province (X. X. Lu et al., 2021). More extreme rainfall events, characterized by abrupt and shorter duration episodes, were observed in the GBA urban areas than in the surrounding regions (Yan et al., 2020).

Numerical simulations have been widely used to explore the urbanization impact on precipitation (Kim et al., 2014; H. Li et al., 2019; Stjern et al., 2011; Zhou & Chen, 2018). By numerically simulating two extreme precipitation events in Atlanta, Shem and Shepherd (2009) indicated that the area with the maximum rainfall increment caused by the UHI effect was located downstream of the city, with rainfall increment by 10%–13%. L. Yang et al. (2014) studied the impact of urbanization on heavy rainfall in the Milwaukee-Lake Michigan region and found that the urbanization altered the energy distribution in the urban region, and the lake breeze and inland wind enhanced the formation of a convergence zone, resulting in a significant increase in rainfall.

Numerical simulations have also been used to study the mechanisms of urban precipitation in China. Guo et al. (2006) used a mesoscale model to investigate the effect of urbanization on the cloud structure and precipitation distribution in Beijing. Their findings revealed that the center of high rainfall intensity was located in the downstream area of the city. Additionally, Yu and Liu (2015) found that urbanization caused an increase in rainfall in Beijing's downstream areas, and a more concentrated spatial distribution of rainfall. Similarly, a high-resolution numerical experiment in the GBA region, one of the most rapidly expanding urban clusters in China, showed significant changes in regional rainfall patterns (J. Wang et al., 2012). Extreme rainfall intensity, spatial distribution, and frequency were found to be very sensitive to the urban surface heat flux (Fung et al., 2021). Results from numerical model experiments also indicated that stronger anthropogenic heat (AH) had led to stronger and more frequent extreme rainfall in the GBA metropolitan areas (Fung et al., 2021; Holst et al., 2016, 2017).

Previous studies have explored the possible mechanisms responsible for urban precipitation changes. Some studies revealed that increased local moisture convergence and vertical motion in and around the city caused by the urban-rural land cover contrast modified the precipitation over or near the city (Niyogi et al., 2011; Shem & Shepherd, 2009; Simpson et al., 2008). Huff and Changnon (1973) proposed four potential pathways for urban precipitation modification. They are (a) a thermal effect due to atmospheric instability over the urban area; (b) a barrier effect caused by the increased mechanical turbulence in the lower boundary layer and possible airflow obstruction around the urban area; (c) urban aerosol effects modified by aerosols and pollution, which lead to changes in the heating profiles, clouds and microphysical process over urban areas; (d) anthropogenic sources such as cooling towers and urban evaporation from greenspaces alter the lower boundary layer moisture and thermal characteristics. The main mechanisms responsible for urban precipitation changes may differ between different cities. For example, Chow and Chang (1984) listed three of those effects, excluding AH, as possible mechanisms for precipitation changes in Shanghai. Surface processes may be important drivers of rainfall changes in the Milwaukee-Lake Michigan region, where cloud aerosol properties over the urban area remained unchanged (L. Yang et al., 2014). For some heavy rainfall in Baltimore, Maryland, and Washington, DC region, aerosols were found to be more influential than UHI (Ntelekos et al., 2008).

The GBA, a megalopolis in China, is frequently attacked by TCs, which usually bring enormous rainfall over the region. While previous studies have shown that urbanization greatly influences precipitation in or near urban areas, the effects of urbanization on urban precipitation due to landfalling TCs in the GBA have not been extensively explored. Therefore, in this study, we attempt to investigate the effects of urban expansion and AH

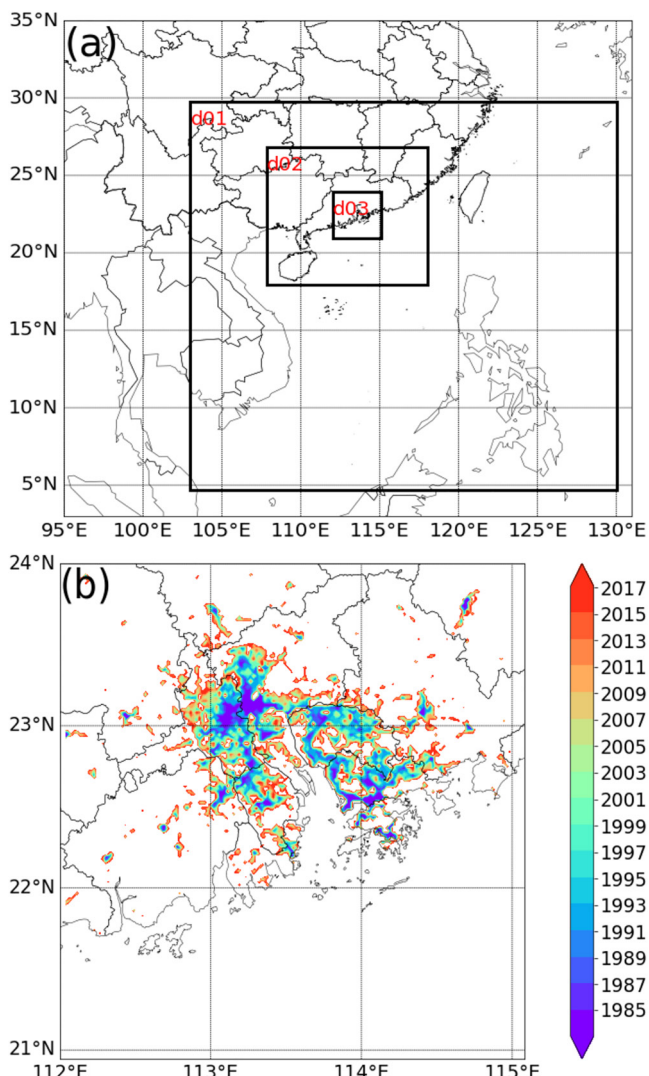


Figure 1. (a) Nested domains for the Weather Research and Forecasting simulation. (b) Urban extension in the D03 covering the Greater Bay Area during 1985–2017.

and has been chosen as a major data source for meteorological, hydrological, and other studies worldwide (J. Wang et al., 2015).

2.2. Model Configuration

The Advanced Research WRF model (Version 3.8.1) coupled with the Urban Canopy Model (UCM) and the Noah Land Surface Model is used to investigate the effects of urban expansion and AH change on TCP in the GBA. The dynamical downscaling for the WRF simulation is performed using three nested domains with one-way nesting. Figure 1a depicts the model domains: Domain 1 (D01) with a horizontal grid spacing of 18 km, Domain 2 (D02) with a grid spacing of 6 km, and Domain 3 (D03) with a grid spacing of 2 km. They cover the East Asia/Western North Pacific area ($4.9\text{--}29.8^{\circ}\text{N}$, $103\text{--}130^{\circ}\text{E}$), South China ($18\text{--}27^{\circ}\text{N}$, $108\text{--}118^{\circ}\text{E}$), and the GBA ($21\text{--}24^{\circ}\text{N}$, $112.5\text{--}115^{\circ}\text{E}$), respectively. The WRF model is configured with 50 levels in the vertical from the surface to 50 hPa. Figure 1b shows the urbanization evolution from 1985 to 2017.

The choice of cumulus parameterization and cloud microphysics schemes in the WRF greatly influence precipitation simulations (Y. Zhang et al., 2021). In this study, the Kain-Fritsch cumulus scheme (Kain & Fritsch, 1993)

enhancement on TCP in the GBA by using the Weather Research and Forecasting Model (WRF). By simulating TCP processes under various degrees of urban expansion and AH values, we aim to explore the mechanisms of AH and urban expansion effects on urban TCP, and compare the different impacts of AH enhancement and urban expansion on environmental factors.

2. Data and Methodology

2.1. Study Area and Data

The GBA comprises nine cities, including Guangzhou, Foshan, Shenzhen, Zhuhai, Dongguan, Zhongshan, Huizhou, Jiangmen, Zhaoqing, and two special administrative regions of Hong Kong and Macau (Figure 1). Over the past few decades, this region has experienced substantial economic growth and rapid urban expansion, making it one of the most urbanized areas in the world. To reflect the process of urbanization, we have applied land use data for urbanization development in the GBA region from 1985 to 2017.

Considering the importance of the urban impervious surface area in characterizing urban built-up areas and urban boundaries (Gong et al., 2020), the urbanization data over this region from 1985 to 2017 is obtained from the Annual maps of global artificial impervious area (GAIA, Gong et al., 2020). Referring to C. X. Hu et al. (2021), all urban grid points are categorized as “urban and built-up land.” During the 32 years, the urban and built-up areas have grown significantly, with a total urban increase of 375% (Figure 1). It is worth mentioning that the GBA is in the monsoonal climate zone, with annual mean temperatures ranging from 21 to 21.3°C and an annual average rainfall of around 1,600 mm accumulated over 130 rainy days (X. Wang et al., 2014).

The data used in this study consists primarily of TC best track data and precipitation data. The TC best track data set, which includes the TC center location (longitude, latitude), minimum central pressure, and the maximum sustained wind speed near the TC center, is provided by the China Meteorological Administration (CMA, X. Q. Lu et al., 2021). The TC best track data sets from the Japan Meteorological Agency (JMA) and the Joint Typhoon Warning Center (JTWC) are also used in this study as references. To validate the numerical simulations of urban rainfall, satellite-based TRMM data at 0.25° grid spacing from TRMM3B42V7 (Huffman et al., 2007) is selected. This data set has been widely used in various regions for comparisons with data from rain gauges and weather radars (Han et al., 2012; Z. Hu et al., 2018)

Table 1
Weather Research and Forecasting (WRF) Physical Parameterization Schemes Used in This Study

Physical process	Parameterization scheme
Microphysics	WRF single-moment 6-class microphysics scheme
Cumulus parameterization	Kain-Fritsch cumulus scheme (only for the D01)
Boundary layer scheme	Yonsei University scheme
Longwave radiation	Rapid Radiative Transfer Model (RRTM) scheme
Shortwave radiation	Dudhia scheme
Surface layer	The Noah land surface model
Urban physical process	Single-layer urban canopy model (SLUCM)

is employed in D01. No cumulus parameterization scheme is used in the inner nested meshes (D02 and D03). We choose the WRF single-moment 6-class microphysics scheme (Hong et al., 2006) as the microphysics scheme for grid-scale cloud and precipitation processes. Note that in the coastal urban agglomeration of the GBA, air-sea interaction has a significant impact on the regional climate; hence a physical option of “sst_update” is enabled. Other physical parameterizations are shown in Table 1.

The basic WRF model can be combined with the UCM for urban weather simulation, as WRF does not fully include urbanization characteristics (Y. Zhang et al., 2014). The Noah land surface model is coupled with a Single-layer urban canopy model to facilitate the simulation of the urban thermal and dynamical interactions (F. Chen et al., 2011; X. Wang et al., 2014). Following the previous study on the urban effect on extreme rainfall in the GBA (C. X. Hu et al., 2021), we use the UCM parameters listed in Table 2. Here AH follows a simple diurnal variation, with peaks in the late morning and late afternoon to evening, and lower values during nighttime, which represents the typical diurnal cycle of human activities in the GBA (Holst et al., 2016). Both sensible and latent heat fluxes (LHF) are simulated, and the ratio of the sensible/latent AH is the default setting value for “urban and built-up land” in the WRF model, which is 2:1.

The horizontal model coordinates are projected using the Lambert conformal map projection. The initial and boundary conditions are provided by National Centers for Environmental Prediction (NCEP) GDAS/FNL 0.25 Degree Global Tropospheric Analyses and Forecast Grids (2022) of the NCEP with 0.25° grid spacing and 6-hr time interval.

2.3. Case Selection and Experimental Design

For the numerical simulation experiments, we choose two TCs: Hato (2017) and Mangkhut (2018), making landfall and affecting the GBA significantly (Choy et al., 2020; J. Yang et al., 2019). The landing times of the two TCs are 0400 UTC on 23 August 2017, and 0900 UTC on 16 September 2018, respectively.

Table 2
Configuration Parameters for Urban Canopy Model (UCM)

UCM parameter	Configuration values
Diurnal maximum anthropogenic heat (W/m ²)	300
Building height (m)	30
Urban fraction	0.9
Standard deviation of roof height (m)	4
Roof width (m)	9.4
Road width (m)	16
Surface albedo of road	0.2
Surface albedo of roof	0.2
Surface albedo of building wall	0.2

To investigate the effect of urban expansion on TCP, we conduct 18 sets of numerical experiments with different underlying surface conditions, that is, NO_Urban, 1985, 1987, 1989, 1991, 1993, 1995, 1997, 1999, 2001, 2003, 2005, 2007, 2009, 2011, 2013, 2015, 2017. For the NO_Urban experiment, we replace all grid points with urban land use in the GBA with cropland, referring to Huang et al. (2019). To quantify the degree of urban expansion, an urbanization expansion coefficient (UEC) is introduced here and is defined as the urban area in a given year divided by the urban area in 2017. The diurnal maximum value for AH is set at 300 W/m² for the urban area. In addition, we set the underlying surface condition to be the land-use condition in 2017, but use different diurnal maximum AH values of 0, 30, 60, 90, 120, 150, 180, 210, 240, 270, 300, 330, 360, 390, 420, 450, 480, 510, 540, 570, 600 W/m² to examine the TCP changes in response to the AH change over the GBA. The underlying surface conditions of 2017 and the diurnal maximum AH value of 300 W m⁻² (Wong et al., 2015) are close to the actual situation for simulating

TCs Hato and Mangkhut and the experiments using the 2017 urbanization data and the diurnal maximum AH value of 300 W m^{-2} are called the control simulations (CTL).

This study focuses on the urbanization effect on TCP in the GBA during TC landfall. Following previous studies (Feng & Shu, 2018; Shu et al., 2021), we investigate the TCP characteristics from 18 hr prior to TC landfall to 24 hr after TC landfall. To simulate the TC landfall well and reduce the error caused by the initial conditions to the uncertainty of the physical quantities of the model (T. Yang et al., 2018), the model begins to run at almost 24 hr prior to TC landfall, and ends at around 24 hr after TC landfall. The first six-hour model runs are considered model spin-up and thus are not included in our following analysis (Kain et al., 2010).

We use the Pearson correlation coefficient to analyze the specific relevance between the UEC/AH series (representing the urbanization level induced by urban expansion and AH enhancement, respectively) and the corresponding TCP (or other related meteorological variables) series over the GBA from the sensitivity experiments. We measure the statistical significance of the correlations using a two-sided Student's *t*-test, where a *p*-value of 0.05 is considered statistically significant (Fisher, 1955). For a sample size of 21/18, an absolute value of correlation coefficient $>0.433/0.468$ is considered significant based on a *p*-value of 0.05.

It is worth mentioning that we calculate the influence of urban expansion and AH enhancement on the variations of TCP and other related meteorological variables over the urban area by using the outputs from D03, while we use the output from D02 to show the correlation between UEC, AH and TCP over the surrounding area of the GBA to demonstrate the wind field and precipitation characteristics over the surrounding area of the GBA.

2.4. Calculation of the Vertically Integrated Moisture Flux Divergence

To explore the environmental background characteristics related to the local rainfall, we calculate the vertically integrated moisture flux divergence (VIMFD). The formula is as follows (van Zomeren & van Delden, 2007):

$$\text{VIMFD} = \frac{1}{g} \int_{P_s}^{P_t} q \left(\frac{\partial u}{\partial x} + \frac{\partial v}{\partial y} \right) dp \quad (1)$$

where *g* is the acceleration due to gravity, *q* is specific humidity, *p* is air pressure, and *u* and *v* are the meridional and zonal wind components. Specifically, *P_s* (the surface pressure) in Equation 1 is chosen to be 1,000 hPa, as the mean surface pressure in the GBA is close to 1,000 hPa. For the *P_t* (the top pressure), van Zomeren and van Delden (2007) reported that the water vapor existed mainly below 700 hPa and they chose 700 hPa to be *P_t* to compute the VIMFD. However, X. X. Lu et al. (2021) found that the spatial distribution of rainfall in South China during summer was more consistent with the VIMFD of the bottom layer from 1,000 to 925 hPa. Therefore, in this study, we will not ascertain which layer should be *P_t*, but set *P_t* from 700 to 990 hPa at an interval of 10 hPa, and calculate VIMFD from 1,000 hPa to *P_t* to examine how urbanization impacts the moisture flux divergence vertically.

3. Results

3.1. Model Validation

Figure 2 compares the control simulation (CTL, using 2017 urbanization data and the diurnal maximum AH value of 300 W m^{-2}) with the best track data from the CMA, JTWC, and JMA, respectively. The CTL reproduces both the tracks and intensity changes of Hato and Mangkhut reasonably well, compared with the three best track data. Prior to the landfalls, the moving directions and landfall locations in CTL are generally consistent with those from the best track data. In particular, the CTL captures the rapid intensification prior to landfall and the rapid weakening after the landfall of Hato. The simulated peak intensity in terms of the maximum 10-m height wind speed for Hato/Mangkhut is $54/43 \text{ m s}^{-1}$, which is close to those of $51.4/47 \text{ m s}^{-1}$ from the JTWC best track data and $52/48 \text{ m s}^{-1}$ from the CMA best track data. The simulated weakening of the two TCs is consistent with the best track data. Overall, CTL reasonably simulates the tracks of the two TCs and reproduces their observed intensity changes quite well.

The accumulated precipitation between 18 hr prior and 24 after landfall obtained from the TRMM and CTL are compared in Figure 3. In the coastal and land areas over $21\text{--}26^\circ\text{N}$, $108\text{--}117^\circ\text{E}$, the spatial correlation between

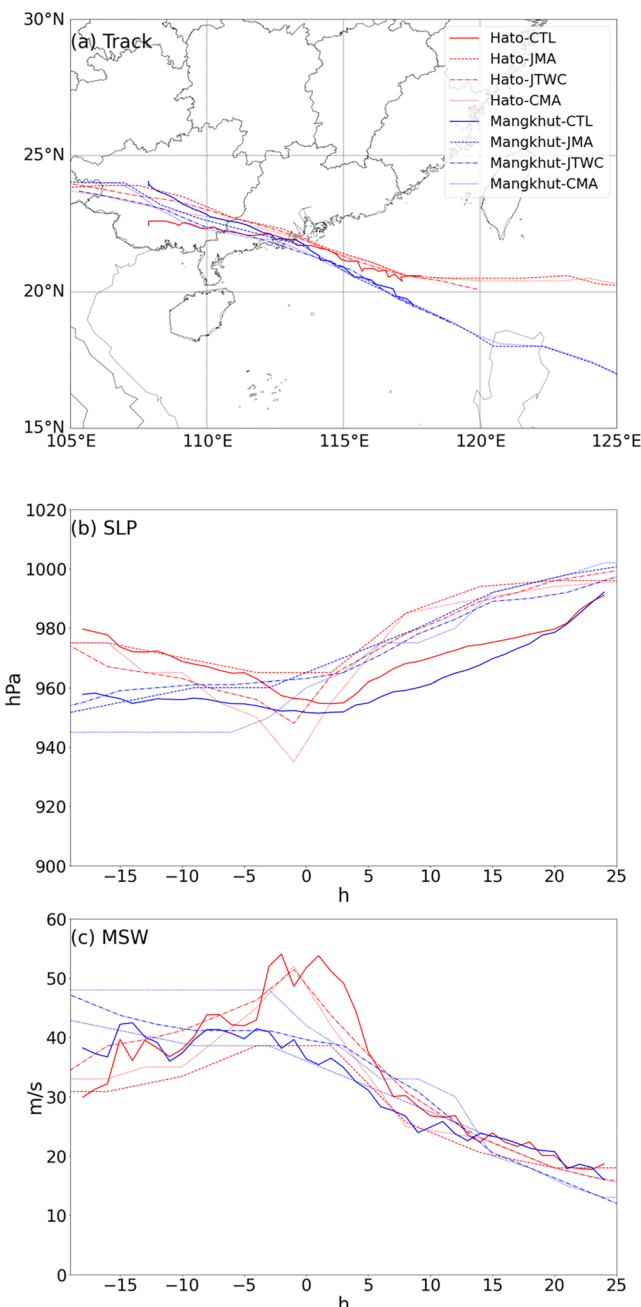


Figure 2. Comparisons between Weather Research and Forecasting (WRF) simulations of the two tropical cyclones (TCs) and the China Meteorological Administration (CMA), Joint Typhoon Warning Center (JTWC), and Japan Meteorological Agency (JMA) best track data for (a) TCs track, (b) central sea level pressure (SLP), (c) maximum sustained wind speed (MSW) near the TC center. The origin of the time on the horizontal axis in (b) and (c) refers to the TC landfall time.

demonstrated in Figure 5a ($p < 0.05$). Figure 5b shows that in the downstream region, there is no significant correlation between TCP and UEC, which is consistent with Figures 4a and 4b. However, a significant positive correlation between TCP and AH is seen in this area (Figure 5b). We can conclude that while both urban expansion and AH enhancement result in an increase in TCP over the urban area, only AH enhancement can increase TCP in the downstream region.

the precipitation by TRMM and CTL is 0.63 for Hato and 0.70 for Mangkhut, respectively, based on the same resolution of 6 km which includes 15,400 grids in total. The average TCPs of Hato/Mangkhut in the coastal and land areas are 51.6/73.7 mm by TRMM and 61.1/94.5 mm by CTL, respectively. There is some discrepancy between the rainfall from CTL and TRMM, which could be attributed to biases in the initial meteorological and boundary conditions, and the imperfect physical parameterization scheme. In addition, Zagrodnik and Jiang (2013) mentioned that TRMM rainfall products might poorly resolve the rain rate in the inner core of a TC. Nonetheless, there is a general consistency in the spatial precipitation distribution between the CTL and observation in the GBA. To further investigate the impact of underlying surface conditions and AH values on the rainfall distribution, sensitivity experiments are conducted by varying these parameters.

3.2. Influence of Urban Expansion and AH Enhancement on TCP

Following the method introduced in Section 2.3, we calculate the correlation coefficients between the TCP variations and the UEC, AH series, respectively, to examine the effects of urban expansion and AH enhancement on TCP in the GBA. The spatial distribution of the correlation between UEC series and the grid TCP series from 1985 to 2017 over the study area is shown in Figures 4a and 4b. The dominant mean wind direction by CTL in the GBA urban area during the TC landfall period is primarily southeasterly, as shown in the figure. In addition, southeast wind prevails in the GBA during the TC peak season (C. Liu et al., 2020; X. X. Lu et al., 2021). Therefore, the northwest direction of GBA is set as the downstream area, which covers about 112.5–114°E, 23–24°N, excluding urban areas, as shown by the blue dash box in Figure 4. In most of the urbanized areas, UEC is positively correlated with the grid TCP significantly (correlation coefficient >0.468 , with a sample size of 18 and $p = 0.05$). However, there is no significant correlation between the grid TCP and UEC over most of the regions in the downstream area of the GBA. Over the downstream area of the GBA during the landfall of Mangkhut, more region with significant negative correlation is found than that with significant positive correlation (Figure 4b).

The spatial distribution of the correlation coefficients between the AH series and the grid TCP series is shown in Figures 4c and 4d. Similar to Figures 4a and 4b, in most of the urbanized GBA areas, AH is positively correlated with TCP significantly (correlation coefficient >0.433 , with a sample size of 21 and $p = 0.05$). It is worth noting that in the downstream region of the GBA, there is a large area with a significant positive correlation between AH and grid TCP, which are different from those shown in Figures 4a and 4b.

We compute the average TCP over the urban GBA region and the downstream region of the GBA based on each of the sensitivity experiments to further explore the relationships between the TCP and urban expansion, AH enhancement. The linear regression fits between the average TCP changes and the UEC, AH series in the two regions are shown in Figures 5a and 5b, respectively. The TCP in the urban region induced by Hato and Mangkhut shows a significant positive correlation with both UEC and AH, as demon-

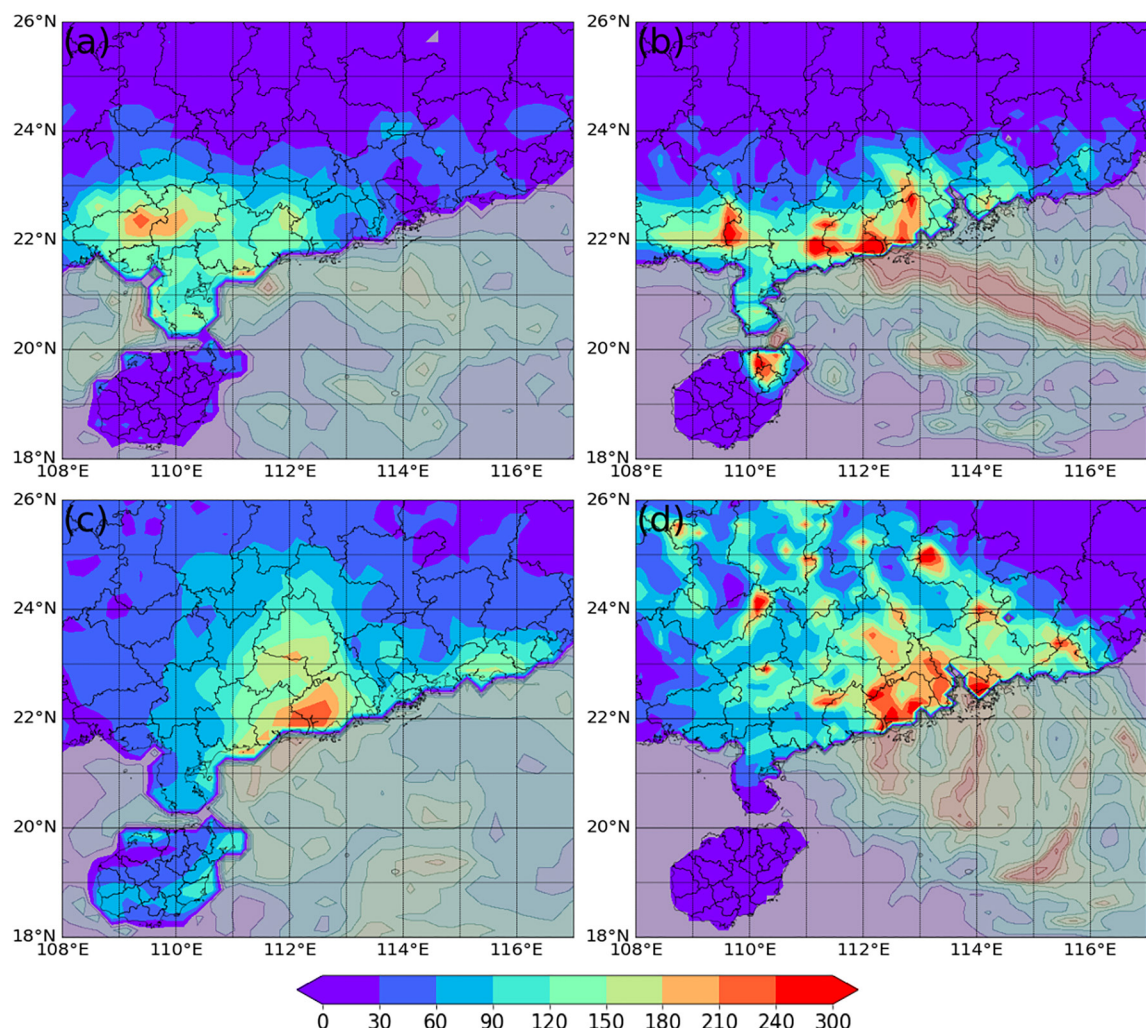


Figure 3. Accumulated tropical cyclone precipitation (TCP) (mm) from 18 hr prior to tropical cyclone (TC) landfall to 24 hr after TC landfall by the Tropical Rainfall Measuring Mission data for (a) Hato and (c) Mangkhut and accumulated TCP (mm) by Weather Research and Forecasting control simulations for (b) Hato and (d) Mangkhut.

3.3. Influence of Urban Expansion and AH Enhancement on Environmental Factors

Surface evaporation, moisture transport, and convection trigger are reported to have an important influence on precipitation in the urban area (Y. Li et al., 2021; Shem & Shepherd, 2009; Y. Zhang et al., 2017). Therefore, in this subsection, we investigate the responses of these environmental factors to urban expansion and AH enhancement in the GBA urban and urban downstream region, attempting to associate these responses with changes in the regional TCP.

3.3.1. Influence on Near Surface Meteorological Factors

We perform linear regressions between UEC, AH series and the regional means of surface LHF (W m^{-2}), temperature at 2-m height (T_2 , $^{\circ}\text{C}$), surface sensible heat flux (SHF, W m^{-2}) over the urban and urban downstream regions from 18 hr prior to TC landfall to 24 hr after TC landfall. Figures 6a and 6b indicate that in both the urban and downstream regions, LHF increases with AH enhancement; however, LHF displays a negative correlation with the UEC in the urban area, while in the downstream region, no significant correlation is found between LHF and UEC. As defined by ECMWF (2022), LHF and surface evaporation are closely related because the transfer of energy that occurs during evaporation is what drives the LHF (Figure S1 in Supporting Information S1). The greater the rate of surface evaporation, the greater the LHF, as more energy is being transferred from the Earth's surface to the atmosphere.

We further analyze the variations of the regional mean T_2 and SHF over the urban area and downstream region, two factors that are often strongly correlated to precipitation (Kusaka et al., 2019). Figures 6c–6f show that T_2

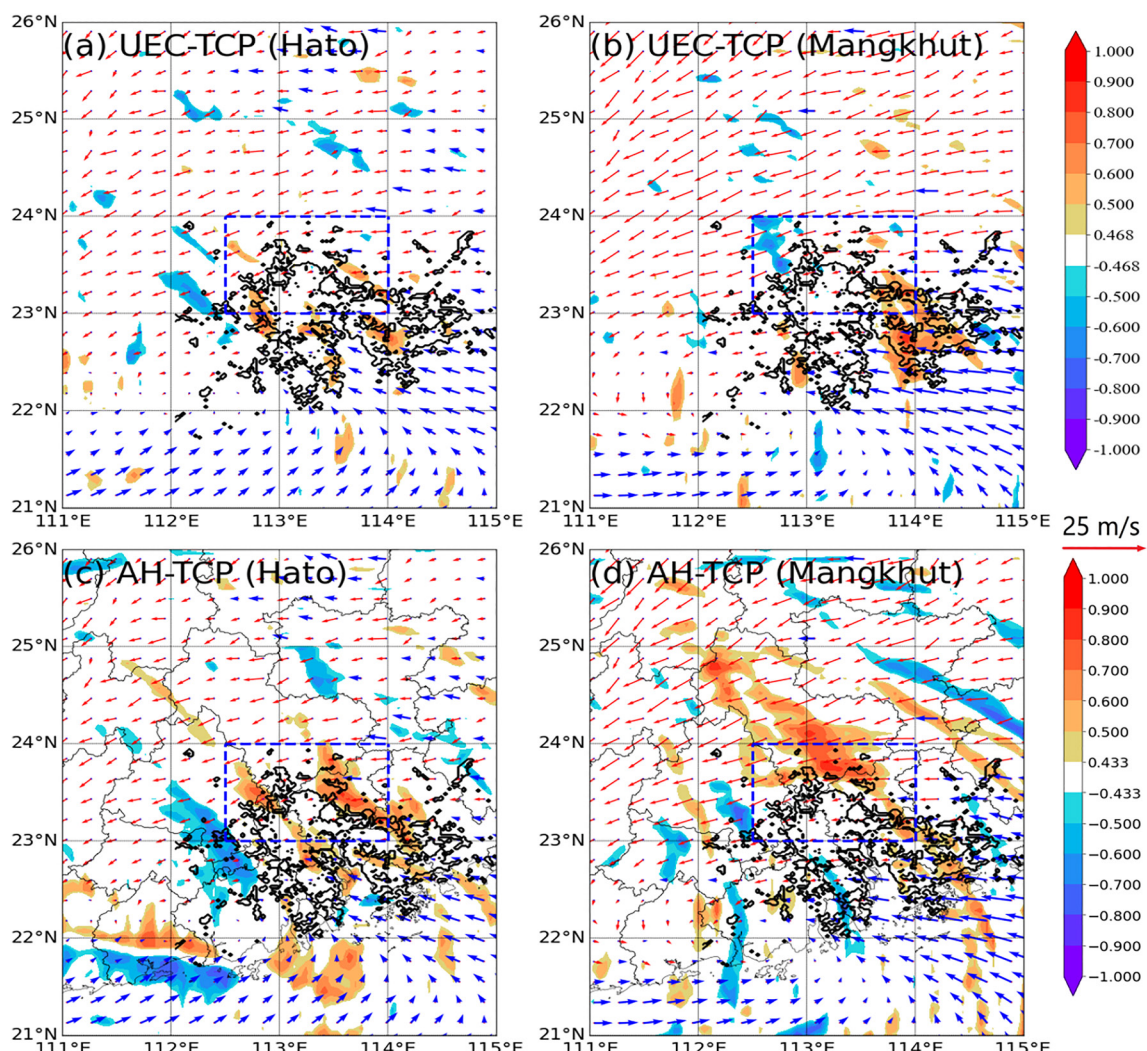


Figure 4. The significant correlation coefficients (shading) between the urbanization expansion coefficient (UEC) series and the grid tropical cyclone precipitation (TCP) series obtained from the sensitive experiments for (a) Hato and (b) Mangkhut, and the significant correlation coefficients (shading) between the anthropogenic heat (AH) series and the grid TCP series obtained from the sensitive experiments for (c) Hato and (d) Mangkhut. The spatial distributions of the average near surface wind from 18 hr prior to tropical cyclone (TC) landfall and 24 hr after TC landfall in the control simulations (CTL) are marked by vectors, where blue (red) vectors denote the southerly (northerly) winds. The Greater Bay Area (GBA) urban area (2017) in CTL is marked by thick black contours, and the blue dash box indicates the downstream area of the GBA, excluding the urban region. Colored shading areas indicate that the correlations are statistically significant ($p = 0.05$).

and SHF in both the urban and downstream regions gradually increase as AH and UEC increase. It is worth noting that the increasing rates of T2 and SHF with AH enhancement and urban expansion are less in the downstream area compared to those in the urban area. According to previous studies (Offerle et al., 2005; Sailor, 2011), urban expansion affects SHF and T2 indirectly by promoting the additional absorption of shortwave radiation and reducing surface reflection, leading to the increase of those two variables, whereas AH enhancement increases SHF and T2 directly. The impact of the increasing temperature in the urban region on rainfall could be either enhancement or abatement, depending on the surrounding environmental background. On the one hand, the increase of SHF and T2 in an urban area may lead to increased water evaporation from the surface, resulting in drier conditions and potentially less rainfall (Rozoff et al., 2003). On the other hand, the increase of SHF and T2 may create more convective activity in the atmosphere with high humidity, which is profit to more rainfall (Carraça & Collier, 2007; Grady & Mote, 2003; Meng et al., 2012; Shepherd & Burian, 2003).

Figure 6a shows that the UEC and AH have different influences on LHF in the urban area. However, Figure 5a shows that UEC and AH positively correlate with the TCP over the urban area. Therefore, the variation pattern of LHF contradicts the TCP change pattern. In addition, Figures 6d and 6f show that UEC and AH have a positive

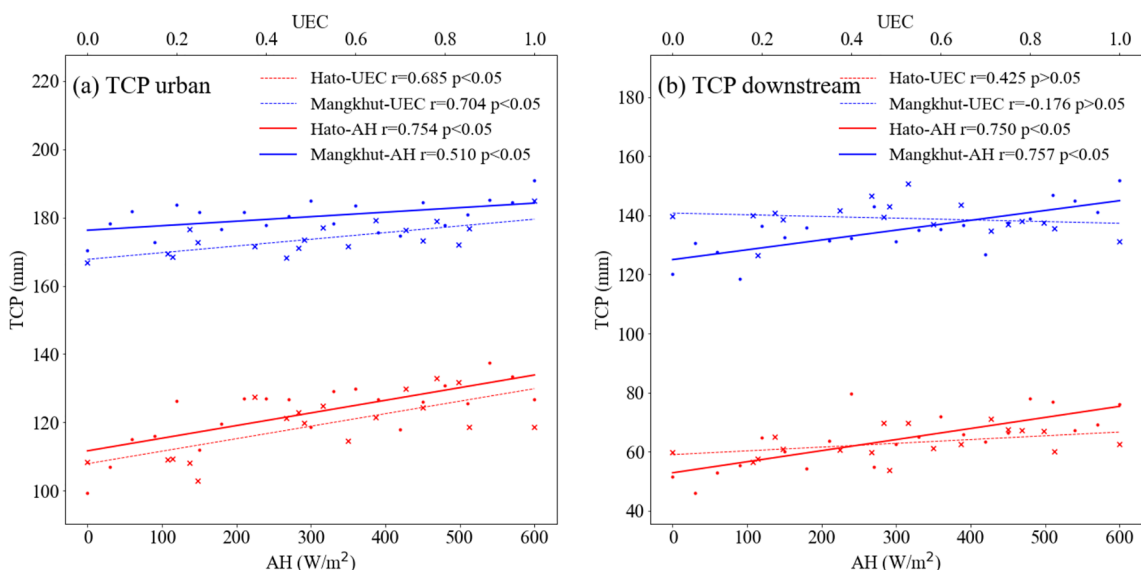


Figure 5. The linear regression fits between the urbanization expansion coefficient (UEC), anthropogenic heat (AH) series and the average tropical cyclone precipitation (TCP) (mm) induced by Hato and Mangkhut based on the sensitivity experiments in (a) the urban region of the Greater Bay Area (GBA) and (b) the downstream region of the GBA. The upper abscissa indicates the UEC scale, and the lower abscissa indicates the AH scale.

relationship with T2 and SHF in the urban downstream area, which differs from the relationship between UEC, AH and TCP over the downstream region, as shown in Figure 5b. Therefore, the variations of LHF, T2 and SHF cannot explain the different TCP changes in the urban and urban downstream areas due to the urban expansion and AH enhancement. Thus, how UEC and AH influence other precipitation-related meteorological factors in the urban and urban downstream areas needs further exploration.

3.3.2. Influence on Moisture Convergence

Moisture transport is one of the most important processes related to regional precipitation (Wen et al., 2020). The precipitation amount is proportional to the VIMFD through the depth of the atmosphere (Banacos & Schultz, 2005; X. X. Lu et al., 2021). To investigate the vertical distribution of the VIMFD changes in response to the UEC and AH variations, we analyze the linear correlation between UEC, AH and VIMFD computed from 1,000 hPa to the top pressure at different heights in the urban and urban downstream regions of the GBA (Figure 7).

As mentioned in the methodology section, we do not ascertain which layer should be Pt (top pressure), but set Pt from 700 to 990 hPa at an interval of 10 hPa, and calculate VIMFD from 1,000 hPa to Pt to examine how urbanization impacts the moisture flux divergence vertically. Figure 7a indicates that there are significant negative correlations between UEC and VIMFD for the top pressure from 760 to 990 hPa for TC Hato (green crossed line) and between UEC and VIMFD for the top pressure from 830 to 990 hPa for TC Mangkhut (blue point line) in the urban region. The maximum correlation between UEC and VIMFD occurs at the top pressure of 900 hPa for both TCs. AH is significantly negatively correlated with VIMFD for the top pressure from 700 to 940 hPa for TC Hato (black triangular line) and for the top pressure from 700 to 910 hPa for TC Mangkhut (red star line). For top pressure from 950 to 990 hPa, no significant negative correlations occur between AH and VIMFD, which may be related to the decreasing specific humidity near 1,000 hPa with AH increase (Fung et al., 2021). The strongest correlation between AH and VIMFD occurs at the top pressure of 850 hPa for both TCs.

Figure 7b shows that in the urban downstream region, there are significant negative correlations between AH and VIMFD for top pressure from 700 to 990 hPa for TC Mangkhut; while for TC Hato, significant correlations are found between AH and VIMFD for the top pressure from 850 to 990 hPa. No significant negative correlation is found between UEC and VIMFD for any top pressure below 700 hPa.

The results suggest that both AH enhancement and urban expansion can increase moisture flux convergence from 1,000 hPa to the top pressure from 850 to 910 hPa in the urban area. AH enhancement favors the moisture flux convergence from 1,000 hPa to the top pressure from 850 to 990 hPa in the urban downstream area, while urban expansion does not have any significant influence. The distribution patterns of VIMFD for the top pressure from

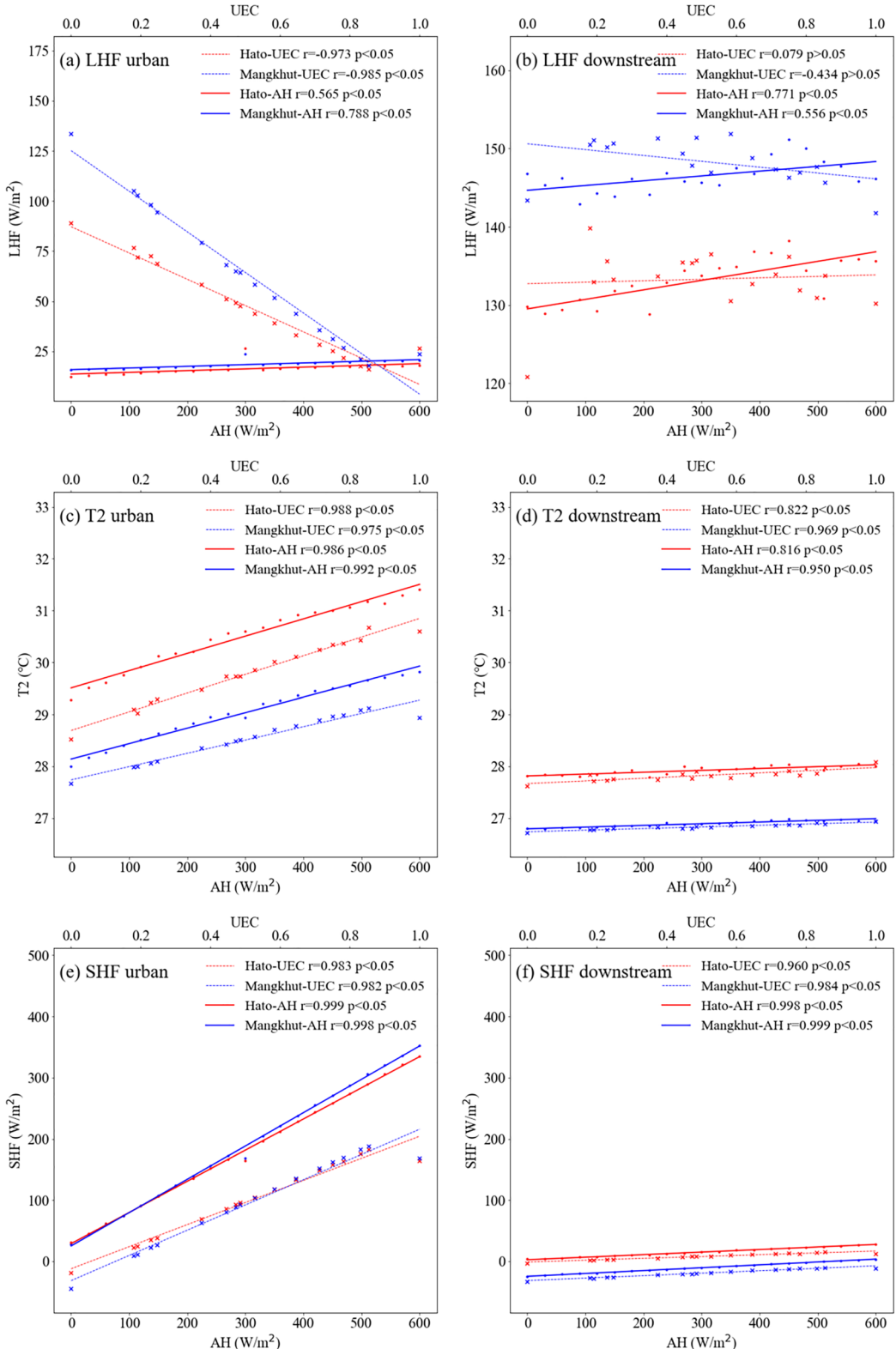


Figure 6.

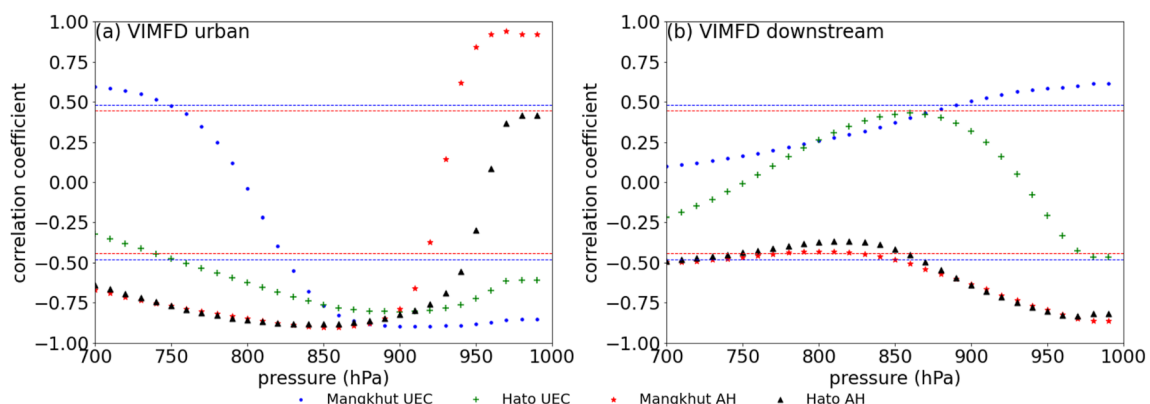


Figure 7. Correlation coefficients between the urbanization expansion coefficient (UEC), anthropogenic heat (AH) and the vertically integrated moisture flux divergence (VIMFD) ($0.01 \text{ g} * \text{m}^{-2} * \text{s}^{-1}$) computed from the ground surface pressure to the top pressure at different levels in (a) urban area (b) urban downstream area. The red/blue horizontal dotted lines in (a) and (b) refer to the thresholds of significant correlation coefficients between AH (21 samples)/UEC (18 samples) and VIMFD ($p = 0.05$).

850 to 910 hPa in urban and urban downstream areas are consistent with the TCP variation patterns shown in Figure 5.

We further explore the spatial distribution of specific humidity at 850 hPa (q850), as q850 is a meteorological factor that is highly correlated to the precipitation (Halder et al., 2015; Liebmann et al., 2017; J. Wang et al., 2018; Wen et al., 2020). Figure 8 depicts the spatial distribution of the correlation coefficients between the UEC, AH series and the grid q850 series in the study area. In the urban region, q850 is significantly positively correlated with the UEC and AH over most of the area, which is consistent with the positive correlation between the TCP and UEC, AH (Figure 5). While in the urban downstream area (the blue dash box region in Figure 8 excluding the urban area) of the GBA, some regions show a significant positive correlation between q850 and AH; however, few areas display a significant correlation between q850 and UEC. These patterns align with TCP observations in Figure 5.

3.3.3. Influence on Atmospheric Stability

Generally, higher Convective Available Potential Energy (CAPE) and lower Convective Inhibition (CIN) are favorable for convection, providing thermodynamic conditions for precipitation (J. Chen et al., 2020; Kirkpatrick et al., 2011; M. Zhang, 2015). Figures 9a and 9b show the linear correlation between the UEC, AH series and CAPE series at 850 hPa in urban and urban downstream regions obtained from the experiments. CAPE has a significant positive correlation with UEC and AH in both urban and downstream regions. Figures 9c and 9d show the linear correlation between the CIN series at 850 hPa in urban and downstream regions obtained from the sensitive experiments and the UEC, AH series. In the urban region, CIN displays a negative correlation with UEC and AH, while in the urban downstream region, no significant correlation is found between UEC, AH and CIN.

In the urban region, more TCP may be related to the increasing CAPE and decreasing CIN with increasing UEC and AH. However, in the downstream region, both UEC and AH have significant positive correlations with CAPE and no significant correlations with CIN. These results indicate that in the downstream region, CAPE and CIN may not be key factors determining the different correlations between TCP and UEC, AH as shown in Figure 5. It is worth mentioning that increasing rates of CAPE with AH enhancement and urban expansion in the downstream area are less than those in the urban area.

3.4. Discussion

The physical mechanisms behind the different responses of TCP to AH enhancement and urban expansion in the urban and downstream areas may be explained in Figure 10. Figure 10a shows that in the urban area, AH

Figure 6. Linear regression fits between urbanization expansion coefficient (UEC), anthropogenic heat (AH) (W m^{-2}) series in the urban area of the Greater Bay Area (GBA) and (a) latent heat flux (LHF) (W m^{-2}), (c) T_2 ($^{\circ}\text{C}$), and (e) sensible heat flux (SHF) (W m^{-2}) series obtained from the sensitive experiments. Linear regression fits between UEC, AH (W m^{-2}) in the urban downstream region of the GBA and (b) LHF, (d) T_2 , and (f) SHF series obtained from the sensitive experiments. The “x” shows the scatter plot between the UEC and the near surface meteorological factors, and the “.” shows the scatter plot between the AH and the near surface meteorological factors. Red color is used to show Mangkhut, and blue color is for Hato.

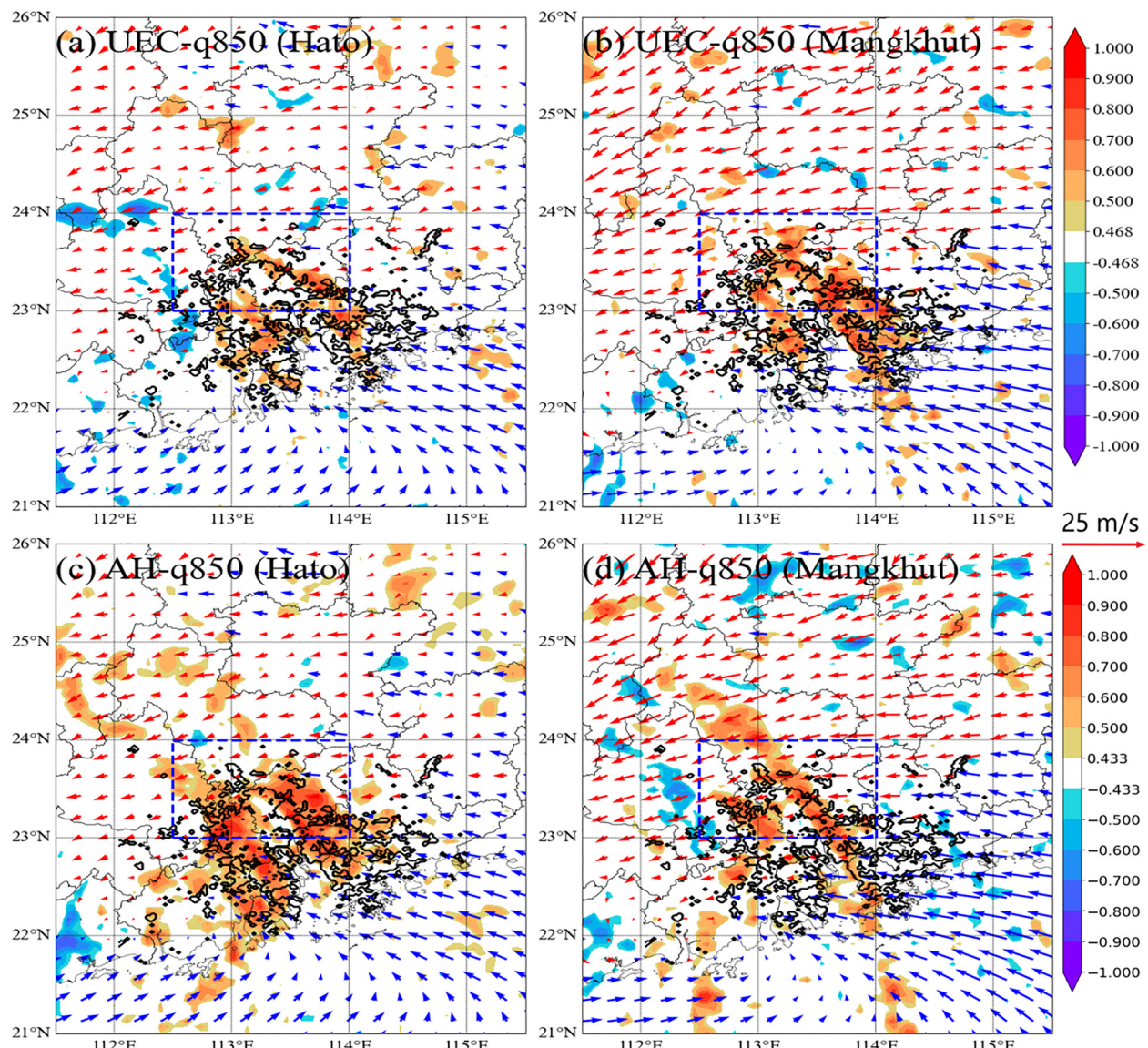


Figure 8. The spatial distribution of the significant correlation coefficients between the grid q850 series (kg kg^{-1}) obtained from the sensitive experiments and urbanization expansion coefficient (UEC) series for (a) Hato, (b) Mangkhut. The spatial distribution of the significant correlation coefficients between the grid q850 series obtained from the sensitive experiments and anthropogenic heat (AH) (W m^{-2}) series for (c) Hato, (d) Mangkhut. The spatial distributions of the average near surface wind during the tropical cyclone landfall period in the control simulations (CTL) are marked by vectors. The Greater Bay Area (GBA) urban area (2017) in CTL is marked by thick black contours, and the blue dash box indicates the downstream area of the GBA, excluding the urban region. The blue (red) vectors denote the southerly (northerly) winds. Colored shading areas indicate that the correlations are statistically significant ($p = 0.05$).

enhancement increases LHF and surface evaporation (Figure 6a), which favors more moisture available. The UHI effect caused by AH enhancement (Figure 6c) increases CAPE (Figure 9a), which represents increased atmospheric instability. The increased availability of moisture from enhanced surface evaporation, along with the enhanced instability due to the UHI effect, leads to an increase in VIMFD in 850–910 hPa (Figure 7a). In addition, there is an increase in the horizontal wind speed in the urban areas, which means more water vapor is transported from the urban area to the downstream area (Figure S2 in Supporting Information S1). In the urban downstream area, increased T2 (Figure 6d), more water vapor transported by horizontal wind from the urban area, more available moisture brought by surface evaporation enhancement (Figure 6b), and increased atmospheric instability (Figure 9b) lead to an enhancement of VIMFD in 850–910 hPa (Figure 7b). Overall, the change patterns of VIMFD in 850–910 hPa with AH enhancement in urban and downstream regions are consistent with changing patterns of TCP.

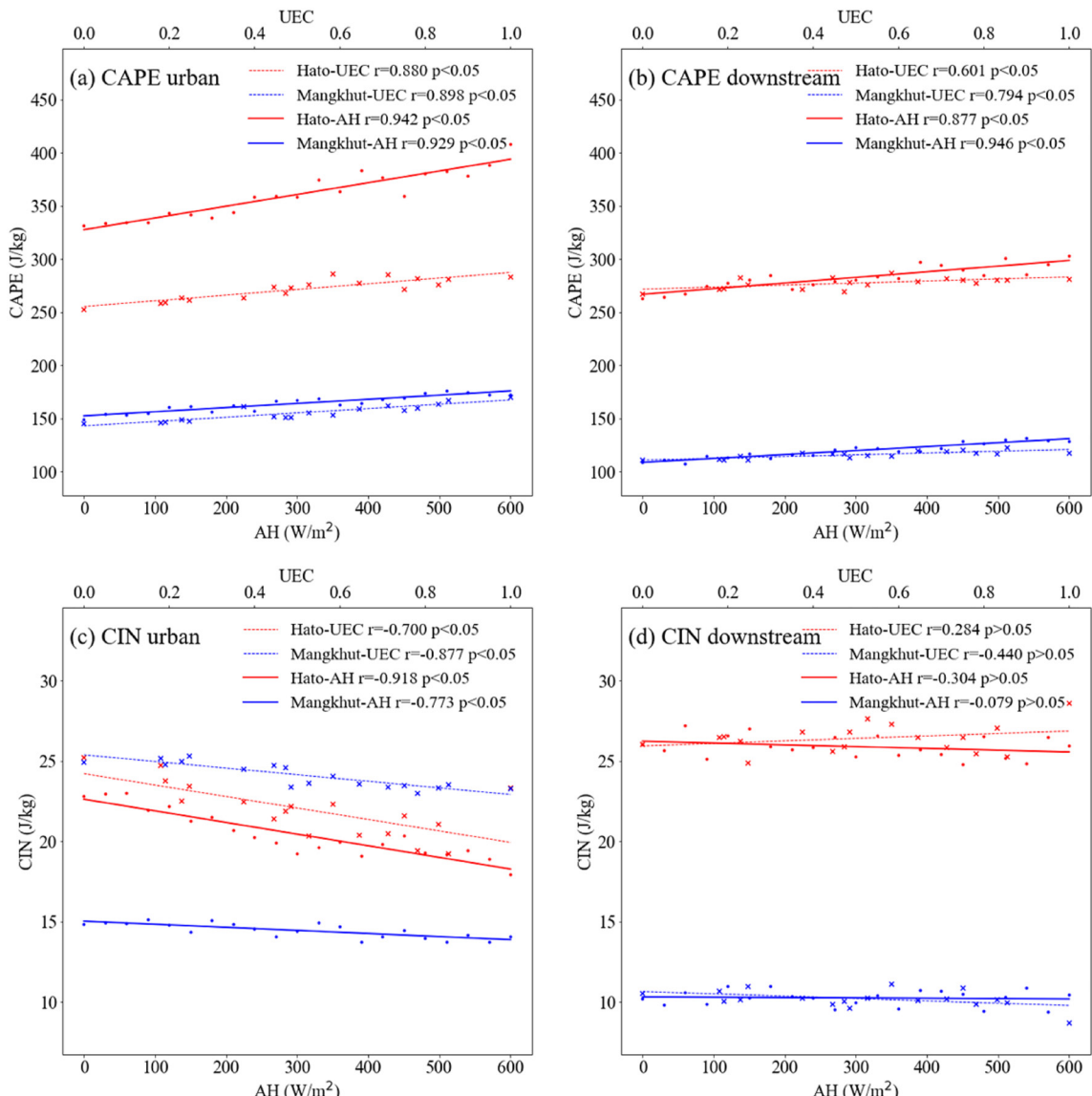


Figure 9. Correlation coefficients between urbanization expansion coefficient (UEC), anthropogenic heat (AH) series and the corresponding atmospheric instability variables series obtained from the sensitive experiments: (a) Convective Available Potential Energy (CAPE) (J kg^{-1}) at 850 hPa in the urban area, (b) CAPE at 850 hPa in the urban downstream area, (c) Convective Inhibition (CIN) (J kg^{-1}) at 850 hPa in the urban area, (d) CIN at 850 hPa in the urban downstream area.

As shown in Figure 10b, in the urban area, urban expansion decreases LHF and surface evaporation (Figure 6a), yielding less moisture available. On the other hand, the UHI effect caused by urban expansion (Figure 6c) increases CAPE (Figure 9a), which represents increased atmospheric instability. With urban expansion, the enhanced friction effect causes increased surface drag, decreasing the near surface wind speed (Figure S2 in Supporting Information S1). The airflow slows down and the resident time of moisture content increases in urbanized areas. These combined effects lead VIMFD in 850–910 hPa (Figure 7a) to increase in the urban area with urban expansion. In addition, the decrease in horizontal wind speed in the urban area means less water vapor is transported from the urban area to the downstream area. In the downstream region, the enhancement of T2 caused by urban expansion is weaker compared to that in urban areas (Figures 6c and 6d). This weaker impact may cause less enhancement of CAPE in the downstream area compared to that in the urban area (Figures 9a and 9b). The decreased moisture transported to the urban downstream area and enhanced atmospheric instability in the downstream area (Figure 9b) have different effects on the moisture flux convergence; therefore, there is an insignificant change in VIMFD in 850–910 hPa (Figures 7b and 10b). Overall, the change patterns of VIMFD in

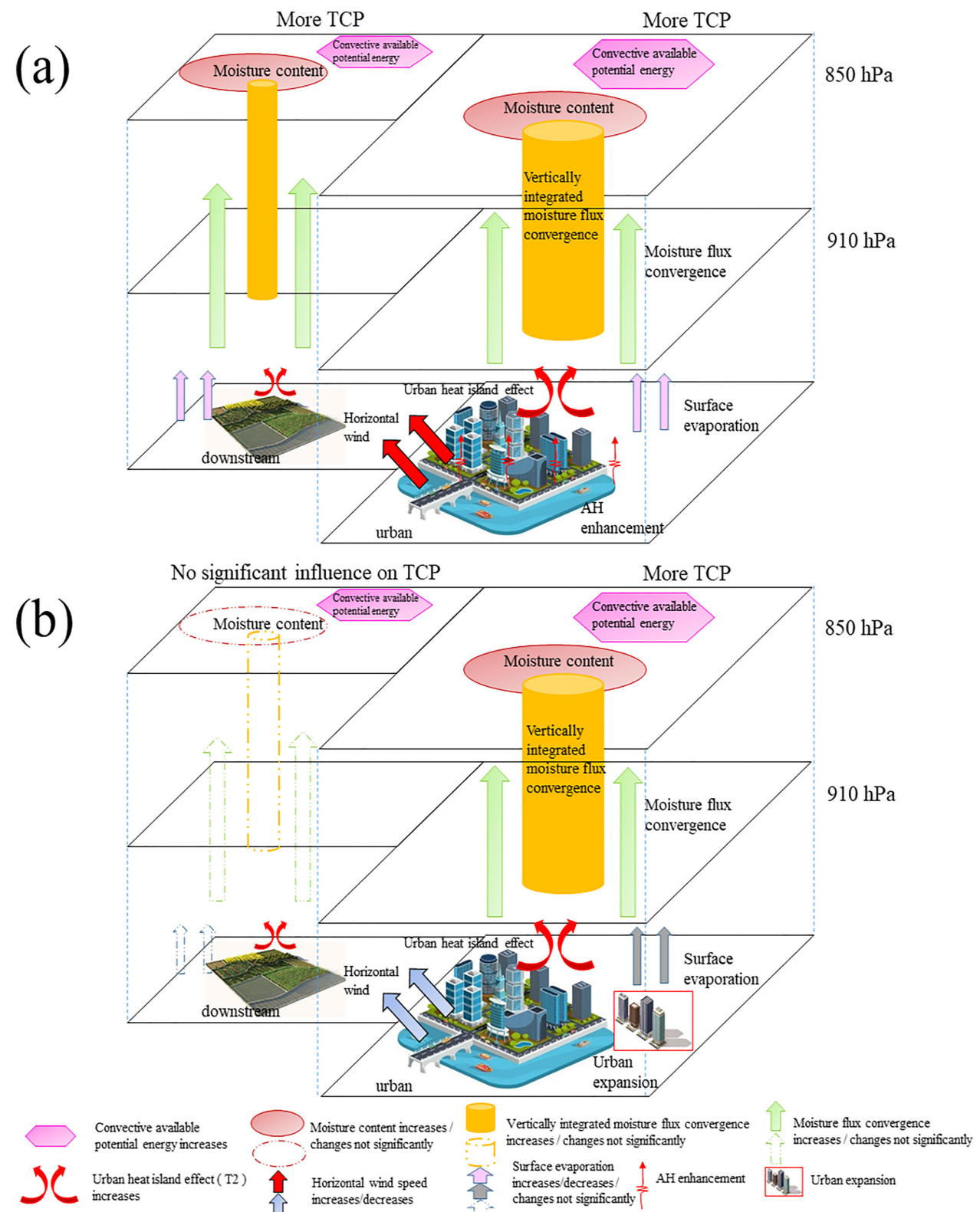


Figure 10. The schematic diagrams of physical mechanisms behind the different responses of tropical cyclone precipitation (TCP) to (a) anthropogenic heat (AH) enhancement and (b) urban expansion. The solid arrows (or lines) in the figure indicate significant changes, while the dashed arrows (or lines) indicate insignificant changes.

850–910 hPa with urban expansion in the urban and downstream regions agree with the change patterns of TCP in the GBA.

4. Conclusions

We have investigated the impact of urban expansion and AH enhancement on TCP in the GBA of China using the WRF-UCM model. Sensitivity experiments are conducted by varying the value of surface AH flux (ranging from 0 to 600 W m^{-2}) and the urban expansion (changing from 1985 to 2017, and including NO_Urban). Two TCs, Hato and Mangkhut that made landfall in or near the GBA, are chosen for the numerical experiments. Results show that the TCP in the urban region would increase with urban expansion and AH enhancement. However, in the urban downstream region, the AH enhancement can cause TCP increase, whereas the urban expansion has no significant influence on TCP.

The near surface meteorological factors, moisture transport, and atmospheric stability are analyzed to explore the mechanisms influencing TCP induced by urbanization in the GBA. In the urban and urban downstream regions, AH enhancement increases LHF and surface evaporation, which may increase moisture availability, while urban expansion does not. The UHI effect, quantified by surface temperature, is enhanced with both AH enhancement and urban expansion. In the urban region, enhanced atmospheric instability, as indicated by increasing CAPE and decreasing CIN, is related to the enhanced UHI effect. In the urban downstream region, the UHI effect is weaker compared to that in urban areas, leading to less enhancement of atmospheric instability. As a result of changes in moisture content and atmospheric instability, the moisture flux convergence between 850 and 910 hPa increases with AH enhancement and urban expansion in the urban region. However, in the urban downstream region, only AH enhancement increases moisture flux convergence between 850 and 910 hPa. Therefore, variations of the low-level moisture convergence, represented by the vertically integrated moisture flux convergence between 850 and 910 hPa, which shows a similar TCP changing pattern, are the key factors influencing the TCP in the urban and urban downstream regions of the GBA.

Data Availability Statement

The CMA best track data (X. Q. Lu et al., 2021; Ying et al., 2014) can be requested from the CMA Tropical Cyclone Data Center. The JTWC and JMA best track data (Knapp et al., 2010, 2018) can be requested from the National Centers for Environmental Information. ERA5 hourly data on pressure levels from 1940 to the present (Hersbach et al., 2023) can be requested from the European Center for Medium-Range Weather Forecasts. NCEP GDAS/FNL 0.25 Degree Global Tropospheric Analyses and Forecast Grids (NCEP, 2015) can be requested from the National Center for Atmospheric Research. Software: All the figures in this manuscript are prepared using Python 3.6 (van Rossum, 2018).

Acknowledgments

This study was supported by the Innovation of Science and Technology Commission of Shenzhen Municipality Ministry with Grants of JCYJ20210324101006016 and GJHZ20210705141403010.

References

- Banacos, P. C., & Schultz, D. M. (2005). The use of moisture flux convergence in forecasting convective initiation: Historical and operational perspectives. *Weather and Forecasting*, 20(3), 351–366. <https://doi.org/10.1175/WAF858.1>
- Carraça, M. G. D., & Collier, C. G. (2007). Modelling the impact of high-rise buildings in urban areas on precipitation initiation. *Meteorological Applications*, 14(2), 149–161. <https://doi.org/10.1002/met.15>
- Changnon, S. A. (1979). Rainfall changes in summer caused by St. Louis. *Science*, 205(4404), 402–404. <https://doi.org/10.1126/science.205.4404.402>
- Chen, F., Kusaka, H., Bornstein, R., Ching, J., Grimmond, C. S. B., Grossman-Clarke, S., et al. (2011). The integrated WRF/urban modelling system: Development, evaluation, and applications to urban environmental problems. *International Journal of Climatology*, 31(2), 273–288. <https://doi.org/10.1002/joc.2158>
- Chen, J., Dai, A., & Zhang, Y. (2020). Linkage between projected precipitation and atmospheric thermodynamic changes. *Journal of Climate*, 33(16), 7155–7178. <https://doi.org/10.1175/JCLI-D-19-0785.1>
- Chow, S. D., & Chang, C. (1984). Shanghai urban influences on humidity and precipitation distribution. *GeoJournal*, 8(3), 201–204. <https://doi.org/10.1007/BF00446468>
- Choy, C. W., Lau, D. S., & He, Y. (2020). Super typhoons Hato (1713) and Mangkhut (1822), part II: Challenges in forecasting and early warnings. *Weather*, 77(9), 324–331. <https://doi.org/10.1002/wea.3746>
- Demuzere, M., Oleson, K., Coutts, A. M., Pigeon, G., & van Lipzig, N. P. M. (2013). Simulating the surface energy balance over two contrasting urban environments using the community land model urban. *International Journal of Climatology*, 33(15), 3182–3205. <https://doi.org/10.1002/joc.3656>
- Dou, J., Wang, Y., Bornstein, R., & Miao, S. (2015). Observed spatial characteristics of Beijing urban climate impacts on summer thunderstorms. *Journal of Applied Meteorology and Climatology*, 54(1), 94–105. <https://doi.org/10.1175/JAMC-D-13-0355.1>
- ECMWF. (2022). Grib parameter database: Parameter details. Retrieved from <https://apps.ecmwf.int/codes/grib/param-db/?id=147>

- Feng, X., & Shu, S. (2018). How do weak tropical cyclones produce heavy rainfall when making landfall over China. *Journal of Geophysical Research: Atmospheres*, 123(21), 11830–11848. <https://doi.org/10.1029/2018JD029228>
- Fisher, R. (1955). Statistical methods and scientific induction. *Journal of the Royal Statistical Society. Series B (Methodological)*, 17(1), 69–78. <https://doi.org/10.1111/j.2517-6161.1955.tb00180.x>
- Fung, K. Y., Tam, C. Y., Lee, T. C., & Wang, Z. (2021). Comparing the influence of global warming and urban anthropogenic heat on extreme precipitation in urbanized pearl river delta area based on dynamical downscaling. *Journal of Geophysical Research: Atmospheres*, 126(21). <https://doi.org/10.1029/2021JD035047>
- Gero, A. F., & Pitman, A. J. (2006). The impact of land cover change on a simulated storm event in the Sydney Basin. *Journal of Applied Meteorology and Climatology*, 45(2), 283–300. <https://doi.org/10.1175/JAM2337.1>
- Gong, P., Li, X., Wang, J., Bai, Y., Chen, B., Hu, T., et al. (2020). Annual maps of global artificial impervious area (GAIA) between 1985 and 2018. *Remote Sensing of Environment*, 236, 111510. <https://doi.org/10.1016/j.rse.2019.111510>
- Grady, D. P., & Mote, T. L. (2003). Patterns and causes of Atlanta's urban heat island-initiated precipitation. *Journal of Applied Meteorology*, 42(9), 1273–1284. [https://doi.org/10.1175/1520-0450\(2003\)042<1273:PACOAU>2.0.CO;2](https://doi.org/10.1175/1520-0450(2003)042<1273:PACOAU>2.0.CO;2)
- Grave, D., Thompson, H. L., Salmon, J. A., Cai, X. M., & Schläfen, K. H. (2013). Modelling the impact of urbanisation on regional climate in the Greater London Area. *International Journal of Climatology*, 33(10), 2388–2401. <https://doi.org/10.1002/joc.3589>
- Guo, X., Fu, D., & Wang, J. (2006). Mesoscale convective precipitation system modified by urbanization in Beijing City. *Atmospheric Research*, 82(1–2), 112–126. <https://doi.org/10.1016/j.atmosres.2005.12.007>
- Halder, S., Dirnmeier, P. A., & Saha, S. K. (2015). Sensitivity of the mean and variability of Indian summermonsoon to land surface schemes in RegCM4: Understanding coupled land-atmosphere feedbacks. *Journal of Geophysical Research: Atmospheres*, 120(18), 9437–9458. <https://doi.org/10.1002/2015JD023101>
- Han, J. Y., Baik, J. J., & Khain, A. P. (2012). A numerical study of urban aerosol impacts on clouds and precipitation. *Journal of the Atmospheric Sciences*, 69(2), 504–520. <https://doi.org/10.1175/JAS-D-11-071.1>
- Hersbach, H., Bell, B., Berrisford, P., Biavati, G., Horányi, A., Muñoz Sabater, J., et al. (2023). ERA5 hourly data on pressure levels from 1940 to present [Dataset]. Copernicus Climate Change Service (C3S) Climate Data Store (CDS). <https://doi.org/10.24381/cds.bd0915c6>
- Holst, C. C., Chan, J. C. L., & Tam, C. Y. (2017). Sensitivity of precipitation statistics to urban growth in a subtropical coastal megacity cluster. *Journal of Environmental Sciences (China)*, 59, 6–12. <https://doi.org/10.1016/j.jes.2017.01.004>
- Holst, C. C., Tam, C. Y., & Chan, J. C. L. (2016). Sensitivity of urban rainfall to anthropogenic heat flux: A numerical experiment. *Geophysical Research Letters*, 43(5), 2240–2248. <https://doi.org/10.1002/2015GL067628>
- Hong, S. Y., Noh, Y., & Dudhia, J. (2006). A new vertical diffusion package with an explicit treatment of entrainment processes. *Monthly Weather Review*, 134(9), 2318–2341. <https://doi.org/10.1175/MWR3199.1>
- Hu, C. X., Fung, K. Y., Tam, C., & Wang, Z. Q. (2021). Urbanization impacts on Pearl River Delta extreme rainfall – Sensitivity to land cover change vs anthropogenic heat. *Earth and Space Science*, 8(3). <https://doi.org/10.1029/2020EA001536>
- Hu, Z., Zhou, Q., Chen, X., Li, J., Li, Q., Chen, D., et al. (2018). Evaluation of three global gridded precipitation data sets in central Asia based on rain gauge observations. *International Journal of Climatology*, 38(9), 3475–3493. <https://doi.org/10.1002/joc.5510>
- Huang, Y., Liu, Y., Liu, Y., Li, H., & Knivell, J. C. (2019). Mechanisms for a record-breaking rainfall in the Coastal Metropolitan City of Guangzhou, China: Observation analysis and nested very large eddy simulation with the WRF model. *Journal of Geophysical Research: Atmospheres*, 124 (3), 1370–1391. <https://doi.org/10.1029/2018JD029668>
- Huff, F. A., & Changnon, S. A. (1973). Precipitation modification by major urban areas. *Bulletin of the American Meteorological Society*, 54(12), 1220–1232. [https://doi.org/10.1175/1520-0477\(1973\)054<1220:pmbmu>2.0.co;2](https://doi.org/10.1175/1520-0477(1973)054<1220:pmbmu>2.0.co;2)
- Huffman, G. J., Adler, R. F., Bolvin, D. T., Gu, G., Nelkin, E. J., Bowman, K. P., et al. (2007). The TRMM multisatellite precipitation analysis (TMPA): Quasi-global, multiyear, combined-sensor precipitation estimates at fine scales. *Journal of Hydrometeorology*, 8(1), 38–55. <https://doi.org/10.1175/JHMS60.1>
- Kain, J. S., & Fritsch, J. M. (1993). Convective parameterization for mesoscale models: The Kain-Fritsch scheme. In K. A. Emanuel & D. J. Raymond (Eds.), *The representation of cumulus convection in numerical models*. Meteorological Monographs (pp. 165–170). American Meteorological Society, Boston, MA. https://doi.org/10.1007/978-1-935704-13-3_16
- Kain, J. S., Xue, M., Coniglio, M. C., Weiss, S. J., Kong, F., Jensen, T. L., et al. (2010). Assessing advances in the assimilation of radar data and other mesoscale observations within a collaborative forecasting-research environment. *Weather and Forecasting*, 25(5), 1510–1521. <https://doi.org/10.1175/2010WAF222405.1>
- Kim, D., Wang, C., Ekman, A. M. L., Barth, M. C., & Lee, D. I. (2014). The responses of cloudiness to the direct radiative effect of sulfate and carbonaceous aerosols. *Journal of Geophysical Research: Atmospheres*, 119(3), 1172–1185. <https://doi.org/10.1002/2013JD020529>
- Kirkpatrick, C., McCaul, E. W., & Cohen, C. (2011). Sensitivities of simulated convective storms to environmental CAPE. *Monthly Weather Review*, 139(11), 3514–3532. <https://doi.org/10.1175/2011MWR3631.1>
- Knapp, K. R., Diamond, H. J., Kossin, J. P., Kruk, M. C., & Schreck, C. J. (2018). International Best Track Archive for Climate Stewardship (IBTrACS) project (Version 4) [Dataset]. NOAA National Centers for Environmental Information. <https://doi.org/10.25921/82ty-9e16>
- Knapp, K. R., Kruk, M. C., Levinson, D. H., Diamond, H. J., & Neumann, C. J. (2010). The International Best Track Archive for Climate Stewardship (IBTrACS) [Dataset]. Bulletin of the American Meteorological Society, 91(3), 363–376. <https://doi.org/10.1175/2009bams2755.1>
- Kusaka, H., Nawata, K., Suzuki-Parker, A., Takane, Y., & Furuhashi, N. (2014). Mechanism of precipitation increase with urbanization in Tokyo as revealed by ensemble climate simulations. *Journal of Applied Meteorology and Climatology*, 53(4), 824–839. <https://doi.org/10.1175/JAMC-D-13-065.1>
- Kusaka, H., Nishi, A., Mizunari, M., & Yokoyama, H. (2019). Urban impacts on the spatiotemporal pattern of short-duration convective precipitation in a coastal city adjacent to a mountain range. *Quarterly Journal of the Royal Meteorological Society*, 145 (722), 2237–2254. <https://doi.org/10.1002/qj.3555>
- Li, H., Zhou, Y., Wang, X., Zhou, X., Zhang, H., & Sodoudi, S. (2019). Quantifying urban heat island intensity and its physical mechanism using WRF/UCM. *Science of the Total Environment*, 650, 3119. <https://doi.org/10.1016/j.scitotenv.2018.10.025>
- Li, Y., Wang, W., Chang, M., & Wang, X. (2021). Impacts of urbanization on extreme precipitation in the Guangdong-Hong Kong-Macau Greater Bay Area. *Urban Climate*, 38, 100904. <https://doi.org/10.1016/j.uclim.2021.100904>
- Liebmann, B., Bladé, I., Funk, C., Allured, D., Quan, X. W., Hoerling, M., et al. (2017). Climatology and interannual variability of boreal spring wet season precipitation in the eastern horn of Africa and implications for its recent decline. *Journal of Climate*, 30(10), 3867–3886. <https://doi.org/10.1175/JCLI-D-16-0452.1>
- Lin, C. Y., Chen, W. C., Chang, P. L., & Sheng, Y. F. (2011). Impact of the urban heat island effect on precipitation over a complex geographic environment in northern Taiwan. *Journal of Applied Meteorology and Climatology*, 50(2), 339–353. <https://doi.org/10.1175/2010JAMC2504.1>

- Liu, C., Li, Q., Zhao, W., Wang, Y., Ali, R., Huang, D., et al. (2020). Spatiotemporal characteristics of near-surface wind in Shenzhen. *Sustainability (Switzerland)*, 12(2), 739. <https://doi.org/10.3390/su12020739>
- Liu, J., & Niyogi, D. (2019). Meta-analysis of urbanization impact on rainfall modification. *Scientific Reports*, 9(1), 7301. <https://doi.org/10.1038/s41598-019-42494-2>
- Lu, X., Li, Q., Chen, S., Zhang, K., Sun, L., Chen, Q., & Zhang, L. (2019). Temporal and spatial precipitation characteristics in Shenzhen from 2008 to 2017. *Advances in Meteorological Science and Technology*, 9(3), 171–178. <https://doi.org/10.3969/j.issn.2095-1973.2019.03.025>
- Lu, X. Q., Yu, H., Ying, M., Zhao, B., Zhang, S., Lin, L., et al. (2021). Western North Pacific tropical cyclone database created by the China Meteorological Administration [Dataset]. Advances in Atmospheric Sciences, 38(4), 690–699. <https://doi.org/10.1007/s00376-020-0211-7>
- Lu, X. X., Li, Q., Zhao, W., Xiao, A., Li, G., & Yu, Z. (2021). Spatiotemporal Characteristics of rainfall in south China from 1967 to 2018. *Journal of Applied Meteorology and Climatology*, 60(9), 1333–1345. <https://doi.org/10.1175/jamc-d-20-0191.1>
- Meng, W., Li, H. R., Zhang, Y., Dai, G., & Wan, Q. L. (2012). A modeling study of the impacts of Pearl River Delta urban environment on convective precipitation. *Chinese Journal of Atmospheric Sciences*, 36(5), 1063–1076. Retrieved from <http://www.iapjournals.ac.cn/dqkx/en/article/doi/10.3878/j.issn.1006-9895.2012.10205>
- National Centers for Environmental Prediction/National Weather Service/NOAA/U.S. Department of Commerce. (2015). NCEP GDAS/FNL 0.25 degree global tropospheric analyses and forecast grids [Dataset]. Research Data Archive at the National Center for Atmospheric Research, Computational and Information Systems Laboratory (updated daily). <https://doi.org/10.5065/D65Q4T4Z>
- NCEP GDAS/FNL 0.25 degree global tropospheric analyses and forecast grids. Research Data Archive at the National Center for Atmospheric Research, Computational and Information Systems. Retrieved from https://www2.mmm.ucar.edu/wrf/users/download/free_data.html
- Niyogi, D., Pyle, P., Lei, M., Arya, S. P., Kishtawal, C. M., Shepherd, M., et al. (2011). Urban modification of thunderstorms: An observational storm climatology and model case study for the Indianapolis urban region. *Journal of Applied Meteorology and Climatology*, 50(5), 1129–1144. <https://doi.org/10.1175/2010JAMC1836.1>
- Ntelekos, A. A., Smith, J. A., Baech, M. L., Krajewski, W. F., Miller, A. J., & Goska, R. (2008). Extreme hydrometeorological events and the urban environment: Dissecting the 7 July 2004 thunderstorm over the Baltimore MD Metropolitan Region. *Water Resources Research*, 44(8), W08446. <https://doi.org/10.1029/2007WR006346>
- Offerle, B., Grimmond, C. S. B., & Fortuniak, K. (2005). Heat storage and anthropogenic heat flux in relation to the energy balance of a central European city centre. *International Journal of Climatology*, 25(10), 1405–1419. <https://doi.org/10.1002/joc.1198>
- Palumbo, A., & Mazzarella, A. (1980). Rainfall statistical properties in Naples. *Monthly Weather Review*, 108(7), 1041–1045. [https://doi.org/10.1175/1520-0493\(1980\)108<1041:RSPIN>2.0.CO;2](https://doi.org/10.1175/1520-0493(1980)108<1041:RSPIN>2.0.CO;2)
- Rozoff, C. M., Cotton, W. R., & Adegoke, J. O. (2003). Simulation of St. Louis, Missouri, land use impacts on thunderstorms. *Journal of Applied Meteorology*, 42(6), 716–738. [https://doi.org/10.1175/1520-0450\(2003\)042<0716:SOSMLM>2.0.CO;2](https://doi.org/10.1175/1520-0450(2003)042<0716:SOSMLM>2.0.CO;2)
- Sailor, D. J. (2011). A review of methods for estimating anthropogenic heat and moisture emissions in the urban environment. *International Journal of Climatology*, 31(2), 189–199. <https://doi.org/10.1002/joc.2106>
- Shem, W., & Shepherd, M. (2009). On the impact of urbanization on summertime thunderstorms in Atlanta: Two numerical model case studies. *Atmospheric Research*, 92(2), 172–189. <https://doi.org/10.1016/j.atmosres.2008.09.013>
- Shepherd, J. M., & Burian, S. J. (2003). Detection of urban-induced rainfall anomalies in a major coastal city. *Earth Interactions*, 7(4), 1–17. [https://doi.org/10.1175/1087-3562\(2003\)007<0001:douira>2.0.co;2](https://doi.org/10.1175/1087-3562(2003)007<0001:douira>2.0.co;2)
- Shimadera, H., Kondo, A., Shrestha, K. L., Kitaoka, K., & Inoue, Y. (2015). Numerical evaluation of the impact of urbanization on summertime precipitation in Osaka, Japan. *Advances in Meteorology*, 2015, 1–11. <https://doi.org/10.1155/2015/379361>
- Shu, S., Feng, X., & Teng, D. (2021). Observed vertical structure of precipitation influenced by dry air for landfalling tropical cyclones over China. *Journal of Geophysical Research: Atmospheres*, 126(11), e2020JD034204. <https://doi.org/10.1029/2020JD034204>
- Simpson, M., Raman, S., Suresh, R., & Mohanty, U. C. (2008). Urban effects of Chennai on sea breeze induced convection and precipitation. *Journal of Earth System Science*, 117(6), 897–909. <https://doi.org/10.1007/s12040-008-0075-1>
- Stjern, C. W., Stohl, A., & Kristjánsson, J. E. (2011). Have aerosols affected trends in visibility and precipitation in Europe? *Journal of Geophysical Research*, 116(2), D02212. <https://doi.org/10.1029/2010JD014603>
- van Rossum, G. (2018). Python tutorial: Release 3.6.6rc1 [Software]. Python Software Foundation. Retrieved from <https://www.python.org/>
- van Zomeran, J., & van Delden, A. (2007). Vertically integrated moisture flux convergence as a predictor of thunderstorms. *Atmospheric Research*, 83(2–4 SPEC. ISS.), 435–445. <https://doi.org/10.1016/j.atmosres.2005.08.015>
- Wang, J., Feng, J., & Yan, Z. (2015). Potential sensitivity of warm season precipitation to urbanization extents: Modeling study in Beijing-Tianjin-Hebei urban agglomeration in China. *Journal of Geophysical Research: Atmospheres*, 120(18), 9408–9425. <https://doi.org/10.1002/2015JD023572>
- Wang, J., Feng, J., & Yan, Z. (2018). Impact of extensive urbanization on summertime rainfall in the Beijing region and the role of local precipitation recycling. *Journal of Geophysical Research: Atmospheres*, 123(7), 3323–3340. <https://doi.org/10.1002/2017JD027725>
- Wang, J., Feng, J., Yan, Z., Hu, Y., & Jia, G. (2012). Nested high-resolution modeling of the impact of urbanization on regional climate in three vast urban agglomerations in China. *Journal of Geophysical Research*, 117(21), 21103. <https://doi.org/10.1029/2012JD018226>
- Wang, X., Liao, J., Zhang, J., Shen, C., Chen, W., Xia, B., & Wang, T. (2014). A numeric study of regional climate change induced by urban expansion in the Pearl River Delta, China. *Journal of Applied Meteorology and Climatology*, 53(2), 346–362. <https://doi.org/10.1175/JAMC-D-13-054.1>
- Wen, J., Chen, J. I., Lin, W., Jiang, B., Xu, S., & Lan, J. (2020). Impacts of anthropogenic heat flux and urban land-use change on frontal rainfall near coastal regions: A case study of a rainstorm over the Pearl River Delta, South China. *Journal of Applied Meteorology and Climatology*, 59(3), 363–379. <https://doi.org/10.1175/JAMC-D-18-0296.1>
- Wong, M. S., Yang, J., Nichol, J., Weng, Q., Menenti, M., & Chan, P. W. (2015). Modeling of anthropogenic heat flux using HJ-1B Chinese small satellite image: A study of heterogeneous urbanized areas in Hong Kong. *IEEE Geoscience and Remote Sensing Letters*, 12(7), 1466–1470. <https://doi.org/10.1109/LGRS.2015.2409111>
- Xiao, Z., Wang, Z., Huang, M., Luo, X., Liang, Y., & Lin, Z. (2020). Urbanization in an underdeveloped City—Nanning, China and its impact on a heavy rainfall event in July. *Earth and Space Science*, 7(4), e2019EA000991. <https://doi.org/10.1029/2019EA000991>
- Yan, M., Chan, J. C. L., & Zhao, K. (2020). Impacts of urbanization on the precipitation characteristics in Guangdong Province, China. *Advances in Atmospheric Sciences*, 37(7), 696–706. <https://doi.org/10.1007/s00376-020-9218-3>
- Yang, J., Li, L., Zhao, K., Wang, P., Wang, D., Sou, I. M., et al. (2019). A comparative study of typhoon Hato (2017) and typhoon Mangkhut (2018)—Their impacts on coastal inundation in Macau. *Journal of Geophysical Research: Oceans*, 124(12), 9590–9619. <https://doi.org/10.1029/2019JC015249>

- Yang, L., Smith, J. A., Baeck, M. L., Bou-Zeid, E., Jessup, S. M., Tian, F., & Hu, H. (2014). Impact of urbanization on heavy convective precipitation under strong large-scale forcing: A case study over the Milwaukee-Lake Michigan region. *Journal of Hydrometeorology*, 15(1), 261–278. <https://doi.org/10.1175/JHM-D-13-020.1>
- Yang, T., Duan, Y., Jing, X., & Feng, J. (2018). Simulation of the urbanization impact on precipitation of landfalling tropical cyclone Nida (2016). *Journal of Applied Meteorological Science*, 29(4), 410–422. <https://doi.org/10.11898/1001-7313.20180403>
- Ying, M., Zhang, W., Yu, H., Lu, X., Feng, J., Fan, Y., et al. (2014). An overview of the China Meteorological Administration tropical cyclone database [Dataset]. *Journal of Atmospheric and Oceanic Technology*, 31(2), 287–301. <https://doi.org/10.1175/jtech-d-12-00119.1>
- Yu, M., & Liu, Y. (2015). The possible impact of urbanization on a heavy rainfall event in Beijing. *Journal of Geophysical Research: Atmospheres*, 120(16), 8132–8143. <https://doi.org/10.1002/2015JD023336>
- Zagrodnik, J. P., & Jiang, H. (2013). Comparison of TRMM precipitation radar and microwave imager rainfall retrievals in tropical cyclone inner cores and rainbands. *Journal of Geophysical Research: Atmospheres*, 118(1), 29–42. <https://doi.org/10.1029/2012JD017919>
- Zhang, C. L., Chen, F., Miao, S. G., Li, Q. C., Xia, X. A., & Xuan, C. Y. (2009). Impacts of urban expansion and future green planting on summer precipitation in the Beijing metropolitan area. *Journal of Geophysical Research*, 114(2), D02116. <https://doi.org/10.1029/2008JD010328>
- Zhang, M. (2015). Numerical models: Coupled ocean-atmosphere models: Physical processes. In *Encyclopedia of atmospheric sciences* (2nd ed.). <https://doi.org/10.1016/B978-0-12-382225-3.00500-4>
- Zhang, Y., Miao, S., Dai, Y., & Bornstein, R. (2017). Numerical simulation of urban land surface effects on summer convective rainfall under different UHI intensity in Beijing. *Journal of Geophysical Research: Atmospheres*, 122(15), 7851–7868. <https://doi.org/10.1002/2017JD026614>
- Zhang, Y., Roundy, J. K., & Santanello, J. A. (2021). Evaluating the impact of model resolutions and cumulus parameterization on precipitation in NU-WRF: A case study in the Central Great Plains. *Environmental Modelling & Software*, 145, 105184. <https://doi.org/10.1016/j.envsoft.2021.105184>
- Zhang, Y., Smith, J. A., Luo, L., Wang, Z., & Baeck, M. L. (2014). Urbanization and rainfall variability in the Beijing metropolitan region. *Journal of Hydrometeorology*, 15(6), 2219–2235. <https://doi.org/10.1175/JHM-D-13-0180.1>
- Zhou, X., & Chen, H. (2018). Impact of urbanization-related land use land cover changes and urban morphology changes on the urban heat island phenomenon. *Science of the Total Environment*, 635, 1467–1476. <https://doi.org/10.1016/j.scitotenv.2018.04.091>